Causal Intervention for Brain tumor Segmentation

Hengxin Liu[1], Qiang Li[1], Weizhi Nie*[2], Zibo Xu[1], and Anan Liu[2]

[1] School of Microelectronics, Tianjin University, Tianjin 300072, China
hengxinliu@tju.edu.cn, liqiang@tju.edu.cn, xzb6666@tju.edu.cn
[2] School of Electrical Automation and Information Engineering, Tianjin University, Tianjin 300072, China
weizhinie@tju.edu.cn, anan0422@gmail.com

Abstract. Due to blurred boundaries between the background and the foreground, along with the overlapping of different tumor lesions, accurate segmentation of brain tumors presents significant challenges. To tackle these issues, we propose a causal intervention model designed for brain tumor segmentation. This model effectively eliminates the influence of irrelevant content on tumor region feature extraction, thereby enhancing segmentation precision. Notably, we adopt a front-door adjustment strategy to mitigate the confounding effects of MRI images on our segmentation outcomes. Our approach specifically targets the removal of background effects and interference in overlapping areas across tumor categories. Comprehensive experiments on the BraTS2020 and BraTS2021 datasets confirm the superior performance of our proposed method, demonstrating its effectiveness in improving accuracy in challenging segmentation scenarios.

Keywords: Brain tumor segmentation · Causal inference · Medical image processing.

1 Introduction

Brain tumors, among the most common and deadly forms of cancer, originate from glial cells and pose a severe threat to human health and life. Magnetic Resonance Imaging (MRI) is extensively used in detecting brain tumors due to its high soft tissue contrast and non-invasive approach. However, manual segmentation of tumors from MRI scans is complex and time-consuming due to the tumors' variable sizes, shapes, potential locations throughout the brain, and the minor contrast differences between tumorous and healthy tissues [4, 20, 11]. With the advancement of computer technology and deep learning techniques, numerous automated brain tumor segmentation methods have been proposed. These automated segmentation methods can significantly enhance segmentation efficiency, alleviate the burden of clinical doctors, and enable real-time monitoring of brain tumor surgical procedures, thereby ensuring surgical safety [15, 14].

Recent studies focused on deep learning-based approaches for brain tumor segmentation [18, 30, 5, 13, 16]. The nnU-Net [12] framework enhances U-Net architecture with data augmentation, region-specific training, and advanced post-processing to achieve superior segmentation. The DMFNet (Dilated Multi-Fiber Network) [6] reduces model complexity through group convolutions, utilizing dilated convolutions and feature fusion for improving accuracy in tumor segmentation. As Transformer's strong ability to capture long-range dependencies [23, 9], many works have applied Transformers to medical image segmentation and achieved favorable results [28, 21, 26, 19]. The TransBTS [25] combined the Transformer with 3D CNN for spatial feature extraction, leading to notable segmentation performance gains. Despite the significant advancements achieved by these methods, challenges still persist in the task of brain tumor segmentation. For instance, these methods overlook the interference of background and healthy tissue regions in MRI images, as well as overlooking the interactions between different tumor categories.

To tackle the challenges previously mentioned, we propose a novel causal brain tumor segmentation method. The proposed method introduces the intermediate variable R through front-door adjustment to mitigate the confounding effects of MRI images on the segmentation results. The causal method is implemented by the region causality module and the category causality module. The region causality module removes the effect of background and healthy tissue. The category causality module can eliminate interference in overlapping areas of different categories of tumors. These causality modules are designed to mitigate the impact of extraneous information on tumor region feature extraction, thereby enhancing segmentation accuracy.

In summary, the main contributions of this paper can be described as follows:

- We propose a causal approach to brain tumor segmentation that significantly reduces the interference of non-relevant content on tumor region feature extraction, leading to improve segmentation accuracy.
- We propose front-door adjustment to remove the confounder to find the real causal relation between the MRI image and the segmentation mask. The proposed method removes the effect of background and eliminates interference in overlapping areas of different tumor categories.
- Ablation and comparative studies demonstrate the effectiveness of our proposed modules and method. Our method outperforms existing state-of-the-art methods on the BraTS2020 and BraTS2021 datasets.

2 Method

In this paper, we propose a novel cascade causal model to remove the influence of background and the interference between different tumor categories. Fig.1 shows the structure of causal model. X denotes brain MRI image, R denotes all tumor regions, C denotes confounder set, Y denotes segmentation mask of each tumor category.

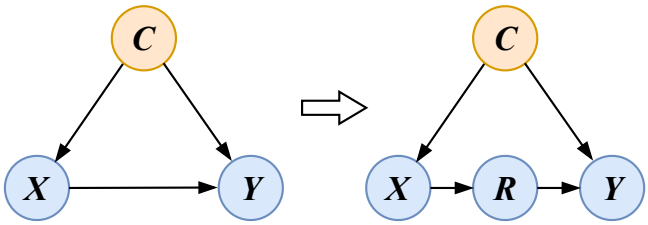

Fig. 1. The causal graph of the tumor segmentation. X denotes brain MRI image, C denotes confounder set, R denotes all tumor regions, Y denotes segmentation mask of each category.

The goal of our work is to learn model's parameters to get $P(Y|X)$. In this step, we hope to remove the confounder to find the real causal relation between X and Y. In order to achieve the goal, we introduce the intermediate variable R, which can be used to build the confounder set and utilize the front-door adjustment to handle the optimization problem.

$$P(Y|X) \approx P(Y|do(X)) = P(R|X)P(Y|do(R)). \tag{1}$$

To estimate $P(Y|do(R))$, we can apply the back-door intervention to cut off the link $R \leftarrow X \leftarrow C \rightarrow Y$. Therefore,

$$\begin{aligned} P(Y|do(R)) &= \sum_c P(Y|do(R), c)P(c|do(R)) \\ &= \sum_c P(Y|R, c)P(c). \end{aligned} \tag{2}$$

Finally, we can calculate $P(Y|do(X))$:

$$P(Y|do(X)) = P(R|X) \sum_c P(Y|R, c)P(c), \tag{3}$$

where, $P(R|X)$ represents that R is achieved from X. R denotes all tumor regions of different categories, which will have obviously relation with Y. There are clear interference items c between the two, such as the background interference mentioned above and the related interference of different tumor categories. In the specific implementation, we designed two modules respectively for $P(R|X)$ and $\sum_c P(Y|R, c)P(c)$. The framework is shown in Fig.2.

2.1 Region Causality Module

In this section, we present the implementation method for $P(R|X)$, introducing the intermediate variable R to ensure the blocking of confounding from X to Y. Given multimodal MRI images X, features are extracted using the encoder of U-Net. Subsequently, a simple segmentation head, comprising a residual block and

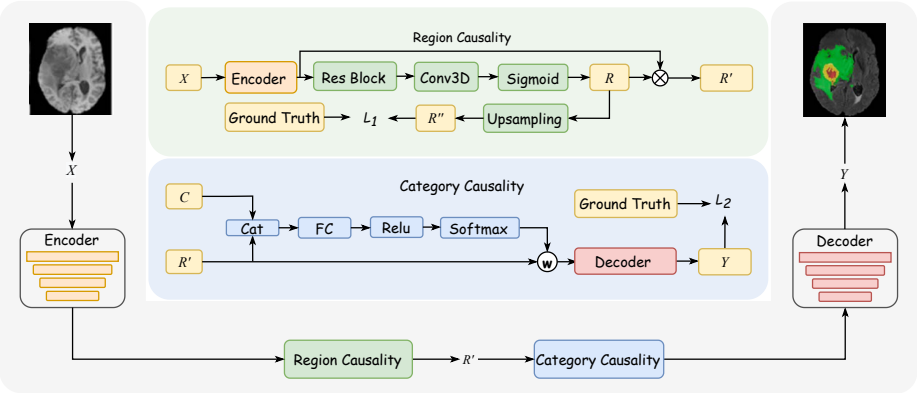

Fig. 2. The architecture of the proposed method. Firstly, the encoder of the U-Net is used to extract the image features. The region causality module obtains a rough segmentation map R from the encoded features through the segmentation head. The rough segmentation map R is multiplied with the encoded features to eliminate confounders and get R'. Then, both the features and the rough segmentation map are input into the category causality module to eliminate category interference. Finally, feature resolution is gradually restored through the decoding path, resulting in the final segmented map.

3D convolution followed by a Sigmoid function, is employed to output tumor regions R of different categories. Multiplying this tumor region of interest by the encoded features yields R', removing the effect of background. Upsample tumor regions R to the size of ground truth to obtain R'', and then compute the loss between R'' and ground truth using the cross-entropy function. By supervising R'', we ensure that R does not contain confounding interference from the background and healthy area.

$$L_1(R'', T) = -\sum_{i=1}^{N}\sum_{k=1}^{K} R''_{i,k}\log(T_{i,k}), \tag{4}$$

where N denotes the number of voxels, K denotes the number of classes, i denotes the index for voxels, k denotes the index for classes, $R'' = R''_{i,k}$ represents the predicted probability map, and $T = T_{i,k}$ represents the ground truth.

2.2 Category Causality Module

The causal intervention $\sum_c P(Y|R,c)P(c)$ was achieved by predicting segmentation mask Y. Because it's challenging to collect all confounders, we approximate it as a fixed confounder dictionary $C = [c_1, ..., c_K]$ to construct the confounder set C in the size of $K \times h \times w \times d$ matrix, where K is the number of categories in the dataset and h, w, d represents the feature dimension of the confounder set. c_k is obtained by averaging the region of tumor features of kth

category. The segmentation network finally computes the probabilities of each tumor category through a Softmax funciton: $P(Y|R,c) = \text{Softmax}(f_y(R,c))$, where $f_y()$ approximates the logits for K tumor categories. Multiplying the encoded features by R yields R', removing the effect of background. Therefore, $P(Y|R,c) = P(Y|R',c) = \text{Softmax}(f_y(R',c))$. And we have

$$P(Y|do(R')) := \mathbb{E}_c\left[\text{Softmax}(f_y(R',c))\right]. \tag{5}$$

Motivated by recent works [24, 22], we can integrate outer expectation into the Softmax function by employing the Normalized Weighted Geometric Mean (NWGM) as:

$$\begin{aligned} P(Y|do(R')) &\approx \text{NWGM}(\mathbb{E}_c\left[\text{Softmax}(f_y(R',c))\right]) \\ &= \frac{\prod_c \exp(f_y(R',c))^{P(c)}}{\sum_{k=1}^{K}\prod_c \exp(f_y(R',c))^{P(c)}} \\ &= \frac{\exp(\mathbb{E}_c\left[f_y(R',c)\right])}{\sum_{k=1}^{K}\exp(\mathbb{E}_c\left[f_y(R',c)\right])} \\ &= \text{Softmax}(\mathbb{E}_c(f_y(R',c))). \end{aligned} \tag{6}$$

The $f_y(R',c)$ is written as linear function $W_1R' + W_2{\cdot}g_y(c)$, where W_1, W_2 denote fully connected layers. We can place $\mathbb{E}$ into the linear function as: $\text{Softmax}(W_1[R'] + W_2\mathbb{E}_c[g_y(c)])$.

We adopt the category attention to explore the interactions between each c in the confounder set C and the tumor region feature R'. Then we can have $\mathbb{E}_c[g_y(c)] = \sum_{k=1}^{K}\text{Softmax}(([R',c_k])P(c_k))R'$, where $P(c_k)$ represents the probability distribution of c_k in dataset. The category causality module is implemented by an attention module as shown in Fig. 2.

Overall loss. As shown in Fig.2, The final segmentation mask is learned under the supervision of ground truth by Dice loss L_2.

$$L_2(Y,T) = 1 - \frac{1}{K}\sum_{k=1}^{K}\frac{2\sum_{i=1}^{N}Y_{i,k}T_{i,k}}{\sum_{i=1}^{N}Y_{i,k} + \sum_{i=1}^{N}T_{i,k}}, \tag{7}$$

where N denotes the number of voxels, K denotes the number of classes, i denotes the index for voxels, k denotes the index for classes, $Y = Y_{i,k}$ represents the predicted final segmentation mask, and $T = T_{i,k}$ represents the ground truth.

The cross-entropy loss L_1 is used to supervise the generation of R''. Consequently, the total loss of the proposed method is expressed as:

$$L = L_1(R'',T) + L_2(Y,T). \tag{8}$$

3 Experiments

3.1 Experimental Setup

We evaluate the segmentation performance of our method on the public BraTS2020 and BraTS2021 datasets[17, 2, 3, 1]. The BraTS2020 dataset consists of a training set of 369 labeled cases and a validation set of 125 unlabeled cases. The

BraTS2021 contains MRI image data from 1251 cases. We divide the BraTS2021 dataset into training, validation, test using a ratio of 4:1:1. Each case has four modalities: T1, T2, T1ce, and FLAIR. The ground truth is labeled by radiologists into four regions: background, enhancing tumor (ET), peritumoral edema (ED), and the necrosis and non-enhancing tumor core (NCR/NET). The segmentation results are evaluated on three regions: enhancing tumor (ET, the enhancing tumor), whole tumor (WT, the sum of peritumoral edema, enhancing tumor, necrotic and non-enhancing tumor), and tumor core (TC, the sum of enhancing tumor, necrotic and non-enhancing tumor). We evaluate the segmentation performance of our method with the Dice score and the Hausdorff Distance (95%) metrics.

Our experiment is operated by Pytorch and trained for 500 epochs using an NVIDIA GeForce RTX 4090 with 24GB memory. We use the Rectified Linear Unit (ReLU) activation function and group normalization, and the batch size is set to 1. We employ Adam optimizer with a learning rate of 0.0001. We apply the following data augmentation methods: random flip, random scale, random cropping, random rotation, and random intensity shift.

3.2 Results and Analysis

Table 1 and Table 2 show the performance comparison of the proposed method with other state-of-the-art methods on the BraTS2020 and BraTS2021 datasets. In Table 1, our method achieves Dice scores of 78.90%, 90.44%, 85.33% and Hausdorff Distances of 26.46mm, 5.43mm, 5.99mm on ET, WT, TC on the BraTS2020 dataset. Compared to TransBTS [25], the Dice scores of proposed method for ET, WT, and TC were higher by 0.17%, 0.35%, and 3.60%, and the Hausdorff Distances for TC were shorter by 3.78 mm. Additionally, compared to other models, our method demonstrated superior performance in the challenging segmentation of tumor core regions. In Table 2, Our method also achieves superior performance with significant improvements. From the experimental results in Table 1 and Table 2, we can see that the proposed method has eliminated the influence of the background on the tumor area and achieved higher segmentation scores in tumor regions. Furthermore, we achieved favorable results across three different tumor regions.

Table 3 presents the ablation study of each module on the BraTS 2020 dataset. RCM denotes the region causality module and CCM represents the category causality module. It can be seen that both the region causality module and the category causality module improved the segmentation results. After adding the region causality module, all performance metrics of the network have improved. The Dice scores increased 1.17%, 0.37%, and 2.46% on ET, WT, and TC. This is because region causality can effectively eliminate the influence of the background region, providing representative information for the segmentation of tumor regions. Employing the category causality module increases the Dice scores of three tumor regions by 2.11%, 0.06%, and 2.56%, respectively. This is because tumor category causality module eliminates interference between dif-

Table 1. Comparison with state-of-the-art methods on the BraTS2020 dataset.

Method	Dice Score (%)			Hausdorff Dist. (mm)		
	ET	WT	TC	ET	WT	TC
3D U-Net [8]	68.76	84.11	79.06	50.98	13.37	13.61
DMFNet [6]	76.41	90.08	81.50	35.17	7.17	12.17
DAU-Net [10]	78.60	89.80	83.00	27.60	5.40	9.80
nnU-Net [12]	78.88	90.38	82.50	32.74	5.35	11.78
TransUNet [7]	78.42	89.46	78.37	**12.85**	5.97	12.84
AugTransU-Net [29]	78.60	89.80	81.90	24.31	5.56	9.56
CH-UNet [27]	78.00	90.00	82.00	26.58	**4.43**	12.35
TransBTS [25]	78.73	90.09	81.73	17.95	4.96	9.77
Ours	**78.90**	**90.44**	**85.33**	26.46	5.43	**5.99**

Table 2. Comparison with state-of-the-art methods on the BraTS2021 dataset.

Method	Dice Score (%)			Hausdorff Dist. (mm)		
	ET	WT	TC	ET	WT	TC
3D U-Net [8]	83.39	89.59	86.28	6.15	**6.18**	11.49
TransBTS [25]	80.35	89.25	85.35	7.83	15.12	8.21
NestedFormer [26]	85.62	90.12	88.18	**6.08**	10.23	6.43
DBTrans [28]	86.70	**92.41**	90.26	6.13	9.84	6.24
Ours	**87.21**	92.32	**91.19**	6.43	13.92	**5.85**

Table 3. Ablation study for different modules on the BraTS 2020 dataset.

Model	RCM	CCM	Dice Score (%)			Hausdorff Dist. (mm)		
			ET	WT	TC	ET	WT	TC
1	-	-	76.04	90.16	82.62	27.56	5.89	6.95
2	+	-	77.21	**90.53**	85.08	32.58	**5.02**	6.14
3	-	+	78.15	90.22	85.18	29.43	5.10	6.21
4	+	+	**78.90**	90.44	**85.33**	**26.46**	5.43	**5.99**

ferent tumor categories, imparting distinctiveness to tumor regions of various categories.

Fig. 3 displays the visual segmentation results on the BraTS2020 dataset. The red, green, and yellow regions represent the peritumoral edema, enhancing tumor and necrosis and non-enhancing tumor. The yellow boxes in the first column of images represent the tumor regions we aim to segment. The blue and red boxes represent the segmentation results of tumor areas by different methods. From the red boxes, it is evident that other methods have incorrectly identified tumor regions as healthy tissue areas, while our method is not affected by the confounding interference of healthy areas on tumor regions, thus successfully identifying the tumor areas. Additionally, as shown by the blue boxes in the first row, other methods mistakenly identify enhancing tumor as necrosis and non-enhancing tumor, while our method mitigates this misjudgment. The blue boxes in the second row reveal that other methods incorrectly recognize edema region

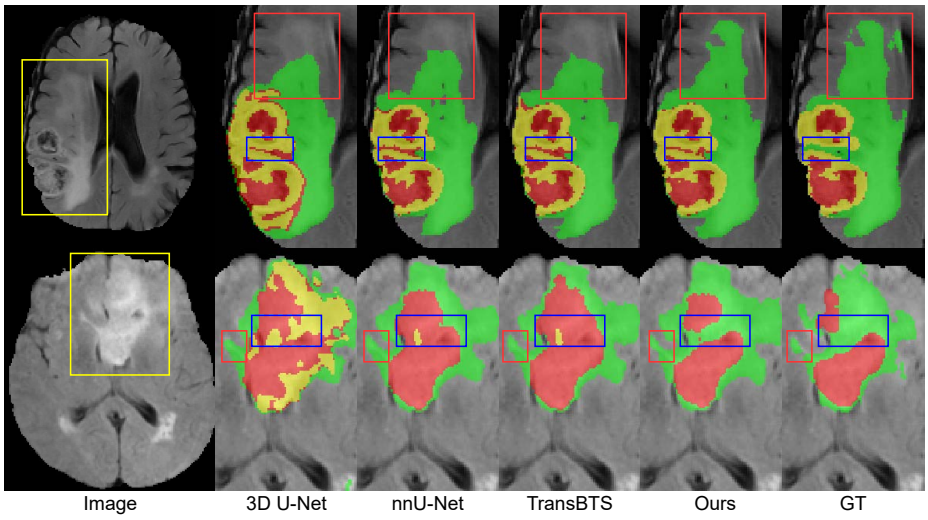

Fig. 3. The visual comparison results on the BraTS2020 dataset. The red region represents the necrosis and non-enhancing tumor; the green region indicates the peritumoral edema; and the yellow region represents the enhancing tumor.

as necrosis and non-enhancing region, while our method accurately distinguishes these two types of regions. Overall, the visualization results demonstrate that our method can segment tumor regions more accurately and distinguish between different types of tumor regions more clearly. This proves that our causal model can effectively eliminate the confounding interference of background and healthy areas on tumor regions, and it can also mitigate the confounding interference between different tumor categories.

4 Conclusion

In this paper, we propose a causal intervention model for brain tumor segmentation. We introduce the front-door adjustment to mitigate the confounding effect. The front-door adjustment is implemented by the region causality module and the category causality module. The proposed method effectively mitigates interference emanating from both background and healthy tissue on tumor regions, and additionally, alleviates interference amongst various tumor categories. The ablation study demonstrates the effectiveness of the region causality module and the category causality module. The visual segmentation results demonstrate the advantages of our proposed causal model in eliminating background interference and interference between tumor categories. Experimental results demonstrate the effectiveness of our proposed method on the BraTS2020 and BraTS2021 datasets. Our proposed causal segmentation method is effective and can be extended to other medical tasks. Our future work will explore the model's robustness across different MRI machines, analyze computational efficiency and

examine the algorithm's performance on the domain generalization problem in MRI segmentation.

Acknowledgments. This work was supported in part by the National Natural Science Foundation of China (62272337).

Disclosure of Interests. The authors have no competing interests to declare that are relevant to the content of this article.

References

1. Baid, U., Ghodasara, S., Mohan, S., Bilello, M., Calabrese, E., Colak, E., Farahani, K., Kalpathy-Cramer, J., Kitamura, F.C., Pati, S., et al.: The rsna-asnr-miccai brats 2021 benchmark on brain tumor segmentation and radiogenomic classification. arXiv preprint arXiv:2107.02314 (2021)
2. Bakas, S., Akbari, H., Sotiras, A., Bilello, M., Rozycki, M., Kirby, J.S., Freymann, J.B., Farahani, K., Davatzikos, C.: Advancing the cancer genome atlas glioma mri collections with expert segmentation labels and radiomic features. Scientific data **4**(1), 1–13 (2017)
3. Bakas, S., Reyes, M., Jakab, A., Bauer, S., Rempfler, M., Crimi, A., Shinohara, R.T., Berger, C., Ha, S.M., Rozycki, M., et al.: Identifying the best machine learning algorithms for brain tumor segmentation, progression assessment, and overall survival prediction in the brats challenge. arXiv preprint arXiv:1811.02629 (2018)
4. Bauer, S., Wiest, R., Nolte, L.P., Reyes, M.: A survey of mri-based medical image analysis for brain tumor studies. Physics in Medicine & Biology **58**(13), R97 (2013)
5. Brügger, R., Baumgartner, C.F., Konukoglu, E.: A partially reversible u-net for memory-efficient volumetric image segmentation. In: Medical Image Computing and Computer Assisted Intervention–MICCAI 2019: 22nd International Conference, Shenzhen, China, October 13–17, 2019, Proceedings, Part III 22. pp. 429–437. Springer (2019)
6. Chen, C., Liu, X., Ding, M., Zheng, J., Li, J.: 3d dilated multi-fiber network for real-time brain tumor segmentation in mri. In: International Conference on Medical Image Computing and Computer-Assisted Intervention. pp. 184–192. Springer (2019)
7. Chen, J., Lu, Y., Yu, Q., Luo, X., Adeli, E., Wang, Y., Lu, L., Yuille, A.L., Zhou, Y.: Transunet: Transformers make strong encoders for medical image segmentation. arXiv preprint arXiv:2102.04306 (2021)
8. Çiçek, Ö., Abdulkadir, A., Lienkamp, S.S., Brox, T., Ronneberger, O.: 3d u-net: learning dense volumetric segmentation from sparse annotation. In: International conference on medical image computing and computer-assisted intervention. pp. 424–432. Springer (2016)
9. Dosovitskiy, A., Beyer, L., Kolesnikov, A., Weissenborn, D., Zhai, X., Unterthiner, T., Dehghani, M., Minderer, M., Heigold, G., Gelly, S., et al.: An image is worth 16x16 words: Transformers for image recognition at scale. arXiv preprint arXiv:2010.11929 (2020)
10. Feng, Y., Cao, Y., An, D., Liu, P., Liao, X., Yu, B.: Daunet: A u-shaped network combining deep supervision and attention for brain tumor segmentation. Knowledge-Based Systems **285**, 111348 (2024)

11. Gordillo, N., Montseny, E., Sobrevilla, P.: State of the art survey on mri brain tumor segmentation. Magnetic resonance imaging **31**(8), 1426–1438 (2013)
12. Isensee, F., Jaeger, P.F., Kohl, S.A., Petersen, J., Maier-Hein, K.H.: nnu-net: a self-configuring method for deep learning-based biomedical image segmentation. Nature methods **18**(2), 203–211 (2021)
13. Liu, Z., Tong, L., Chen, L., Zhou, F., Jiang, Z., Zhang, Q., Wang, Y., Shan, C., Li, L., Zhou, H.: Canet: Context aware network for brain glioma segmentation. IEEE Transactions on Medical Imaging **40**(7), 1763–1777 (2021)
14. Lotlikar, V.S., Satpute, N., Gupta, A.: Brain tumor detection using machine learning and deep learning: A review. Current Medical Imaging (2021)
15. Louis, D.N., Ohgaki, H., Wiestler, O.D., Cavenee, W.K., Burger, P.C., Jouvet, A., Scheithauer, B.W., Kleihues, P.: The 2007 who classification of tumours of the central nervous system. Acta neuropathologica **114**(2), 97–109 (2007)
16. Luo, Z., Jia, Z., Yuan, Z., Peng, J.: Hdc-net: Hierarchical decoupled convolution network for brain tumor segmentation. IEEE Journal of Biomedical and Health Informatics **25**(3), 737–745 (2020)
17. Menze, B.H., Jakab, A., Bauer, S., Kalpathy-Cramer, J., Farahani, K., Kirby, J., Burren, Y., Porz, N., Slotboom, J., Wiest, R., et al.: The multimodal brain tumor image segmentation benchmark (brats). IEEE transactions on medical imaging **34**(10), 1993–2024 (2014)
18. Myronenko, A.: 3d mri brain tumor segmentation using autoencoder regularization. In: International MICCAI Brainlesion Workshop. pp. 311–320. Springer (2018)
19. Peiris, H., Hayat, M., Chen, Z., Egan, G., Harandi, M.: A robust volumetric transformer for accurate 3d tumor segmentation. In: International Conference on Medical Image Computing and Computer-Assisted Intervention. pp. 162–172. Springer (2022)
20. Sharma, N., Aggarwal, L.M.: Automated medical image segmentation techniques. Journal of medical physics/Association of Medical Physicists of India **35**(1), 3 (2010)
21. She, D., Zhang, Y., Zhang, Z., Li, H., Yan, Z., Sun, X.: Eoformer: Edge-oriented transformer for brain tumor segmentation. In: International Conference on Medical Image Computing and Computer-Assisted Intervention. pp. 333–343. Springer (2023)
22. Tian, Y., Bai, K., Yu, X., Zhu, S.: Causal multi-label learning for image classification. Neural Networks **167**, 626–637 (2023)
23. Vaswani, A., Shazeer, N., Parmar, N., Uszkoreit, J., Jones, L., Gomez, A.N., Kaiser, Ł., Polosukhin, I.: Attention is all you need. In: Advances in Neural Information Processing Systems. pp. 5998–6008 (2017)
24. Wang, T., Huang, J., Zhang, H., Sun, Q.: Visual commonsense r-cnn. In: Proceedings of the IEEE/CVF conference on computer vision and pattern recognition. pp. 10760–10770 (2020)
25. Wang, W., Chen, C., Ding, M., Yu, H., Zha, S., Li, J.: Transbts: Multimodal brain tumor segmentation using transformer. In: International Conference on Medical Image Computing and Computer-Assisted Intervention. pp. 109–119. Springer (2021)
26. Xing, Z., Yu, L., Wan, L., Han, T., Zhu, L.: Nestedformer: Nested modality-aware transformer for brain tumor segmentation. In: International Conference on Medical Image Computing and Computer-Assisted Intervention. pp. 140–150. Springer (2022)

27. Xu, W., Yang, H., Zhang, M., Cao, Z., Pan, X., Liu, W.: Brain tumor segmentation with corner attention and high-dimensional perceptual loss. Biomedical Signal Processing and Control **73**, 103438 (2022)
28. Zeng, X., Zeng, P., Tang, C., Wang, P., Yan, B., Wang, Y.: Dbtrans: A dual-branch vision transformer for multi-modal brain tumor segmentation. In: International Conference on Medical Image Computing and Computer-Assisted Intervention. pp. 502–512. Springer (2023)
29. Zhang, M., Liu, D., Sun, Q., Han, Y., Liu, B., Zhang, J., Zhang, M.: Augmented transformer network for mri brain tumor segmentation. Journal of King Saud University-Computer and Information Sciences **36**(1), 101917 (2024)
30. Zhou, T., Canu, S., Vera, P., Ruan, S.: 3d medical multi-modal segmentation network guided by multi-source correlation constraint. In: 25th International Conference on Pattern Recognition. pp. 10243–10250. IEEE (2020)